Electric-field-induced strain contributions in morphotropic phase boundary composition of (Bi1/2Na1/2)TiO3-BaTiO3 during poling

Neamul H. Khansur, Manuel Hinterstein, Zhiyang Wang, Claudia Groh, Wook Jo, and John E. Daniels

Citation: Applied Physics Letters **107**, 242902 (2015); doi: 10.1063/1.4937470

View online: http://dx.doi.org/10.1063/1.4937470

View Table of Contents: http://scitation.aip.org/content/aip/journal/apl/107/24?ver=pdfcov

Published by the AIP Publishing

Electric-field-induced strain contributions in morphotropic phase boundary composition of $(Bi_{1/2}Na_{1/2})TiO_3$-$BaTiO_3$ during poling

Neamul H. Khansur,[1] Manuel Hinterstein,[1,2] Zhiyang Wang,[1,3] Claudia Groh,[4] Wook Jo,[5] and John E. Daniels[1]

[1]*School of Materials Science and Engineering, UNSW Australia, New South Wales 2052, Australia*
[2]*Institute for Applied Materials, Karlsruhe Institute for Technology, P.O. Box 3640, 76021 Karlsruhe, Germany*
[3]*The Australian Synchrotron, Clayton, Victoria 3168, Australia*
[4]*Institute of Materials Science, Technische Universität Darmstadt, Alarich-Weiss-Straße 2, 64287 Darmstadt, Germany*
[5]*School of Materials Science and Engineering, Ulsan National Institute of Science and Technology, Ulsan 44919, South Korea*

(Received 15 September 2015; accepted 27 November 2015; published online 15 December 2015)

The microscopic contributions to the electric-field-induced macroscopic strain in a morphotropic $0.93(Bi_{1/2}Na_{1/2}TiO_3)-0.07(BaTiO_3)$ with a mixed rhombohedral and tetragonal structure have been quantified using full pattern Rietveld refinement of *in situ* high-energy x-ray diffraction data. The analysis methodology allows a quantification of all strain mechanisms for each phase in a morphotropic composition and is applicable to use in a wide variety of piezoelectric compositions. It is shown that during the poling of this material 24%, 44%, and 32% of the total macroscopic strain is generated from lattice strain, domain switching, and phase transformation strains, respectively. The results also suggest that the tetragonal phase contributes the most to extrinsic domain switching strain, whereas the lattice strain primarily stems from the rhombohedral phase. The analysis also suggests that almost 32% of the total strain is lost or is a one-time effect due to the irreversible nature of the electric-field-induced phase transformation in the current composition. This information is relevant to on-going compositional development strategies to harness the electric-field-induced phase transformation strain of $(Bi_{1/2}Na_{1/2})TiO_3$-based lead-free piezoelectric materials for actuator applications. © *2015 AIP Publishing LLC*. [http://dx.doi.org/10.1063/1.4937470]

Among the lead-free piezoelectric ceramics, the bismuth sodium titanate, $(Bi_{1/2}Na_{1/2})TiO_3$ (BNT) based systems have attracted considerable attention, not merely from a potential application point of view but also from a scientific perspective with respect to the fundamental nature of electro-mechanical coupling. Since the first report of BNT, research has been focused on the compositional modifications required to improve its electro-mechanical properties.[1–5] Among them, $(1-x)(Bi_{1/2}Na_{1/2})TiO_3$–$xBaTiO_3$ (BNT-*100x*BT) is considered an attractive system to be investigated as it presents enhanced properties at the morphotropic phase boundary (MPB). Takenaka *et al.*[6] reported an MPB between a rhombohedral and a tetragonal phase in BNT-*100x*BT ($0.06 \leq x \leq 0.07$) system through the electrical property and structure measurements. However, Ranjan and Dviwedi[7] suggested that the crystallographic structure is nearly cubic for BNT-6BT. As yet several phase diagrams for the BNT-*100x*BT system have been reported based on various measurements.[8–12] Nevertheless, it is generally accepted that the MPB of BNT-*100x*BT is situated for $0.06 \leq x \leq 0.11$.

In situ observation of the field-induced structural changes of BNT-*100x*BT by diffraction techniques has shown changes in crystallographic phases. Reports of *in situ* x-ray[13] and neutron[14] diffraction experiments showed that the MPB composition of as-processed BNT-*100x*BT is pseudocubic and undergoes an electric-field-induced phase transformation to tetragonal or mixed phase rhombohedral-tetragonal symmetry. Jo *et al.*[9] have reported phase evolutions in a wide range of BNT-*100x*BT ($0 \leq x \leq 0.15$) compositions at both the unpoled and poled state. Interestingly, despite the results showing the electric-field-induced evolution of mixed phase compositions between BNT-5BT and BNT-11BT, optimal properties were still observed at around BNT-7BT as was reported by Takenaka *et al.*[6] In addition, Ma *et al.*[15] have reported electric-field-induced creation/modification of MPB in this material system by *in situ* TEM. The unusual phase transformation behaviour of BNT-*100x*BT compositions is of interest as it's been shown to provide a mechanism to so-called "giant" strain property or incipient piezoelectricity[16–19] in related BNT-based compositions.

Although structural contributions, such as phase coexistence and non-180° ferroelectric domain switching,[9] to the macroscopic strain are evident in this material, quantitative analysis of microscopic strain contributions is not available. Quantification of the electric-field-induced diffraction data can be useful to get further insights into the structural origin of strain response in piezoelectric materials. For example, it is interesting to understand how individual phases in an MPB composition contribute to the overall macroscopic response. Quantification of microscopic origins from *in situ* diffraction data in different materials has been successfully conducted using selected reflection-fitting methods.[20–24] However, this method to quantify domain texture, lattice strain, and phase transformation strain for mixed-phase materials is difficult due to significant peak overlap. This

difficulty can be overcome using full pattern Rietveld refinements.[25] This refinement strategy enables one to quantify the sources of microscopic contributions to the macroscopic strain by utilizing all available diffraction information. The aim of this work is to reconcile the types of structural contributions present at the microscopic length scales in an MPB composition (BNT-7BT) by quantitative full pattern Rietveld refinements which incorporate texture analysis.

The reported analysis methodology allows a quantification of all strain mechanisms; namely, lattice strain, domain switching strain, and phase transformation strain, for each phase. In contrast to the reported *in situ* neutron diffraction data of a $Pb(Zr,Ti)O_3$-based composition,[25] where small amounts of reversible phase switching occur, here BNT-7BT is shown to have a one-time effect due to the irreversible nature of the phase transformation.

The studied composition $0.93(Bi_{1/2}Na_{1/2}TiO_3)$–$0.07(BaTiO_3)$ (BNT-7BT) was prepared by conventional solid state processing; details can be found elsewhere.[26] Macroscopic strains up to fields of 4 kV/mm were measured with disk-shaped samples by modified sawyer tower setup at a frequency of 50 mHz. Sample dimensions of 0.8 mm $\times$ 1 mm $\times$ 6 mm suitable for *in situ* high-energy diffraction experiments were cut from sintered disks. *In situ* high-energy XRD measurements were carried out at beamline I12-JEEP, Diamond Light Source, UK. A monochromatic x-ray beam of energy 84.82 keV (wavelength, $\lambda = 0.146$ Å) was used in transmission geometry with a large area detector. Using this technique, full orientation dependent data with respect to the angle, ψ, between the scattering vector and applied electric field vector can be collected in a single diffraction image. Diffraction data for one unipolar cycle (maximum electric field, $E_{max} = 4$ kV/mm) in equal steps were collected using a flat-panel Pixium detector.[27–29] The collected diffraction images were radially integrated into 36 azimuthal sections using the software Fit2D.[30] Full pattern Rietveld refinements using the software package MAUD (Materials Analysis Using Diffraction)[31] were performed to describe the structure and domain texture changes as a function of electric field over the entire electrical loading/unloading cycle. The orientation dependent information was extracted using the Exponential Harmonic[32] model and the weighted strain orientation distribution function (WSODF)[33] model.

Figure 1 shows the diffraction pattern of the as-processed BNT-7BT and electric-field-induced changes in the selected diffraction patterns. In the as-processed state, the BNT-7BT composition results in a single phase perovskite type diffraction pattern (Figure 1(a)) that can be indexed with a cubic unit cell. The exact crystallographic structure of the as-processed BNT-7BT is yet to be conclusive. However, previous work has shown that compositions close to the MPB in the BNT-*100x*BT system exist with a long range cubic symmetry but with short range disorder, leading to lower symmetries at the nanometer scale.[34–36] For simplicity, here, the as-processed BNT-7BT has been termed as pseudocubic.

Data presented in Figures 1(b) and 1(c) signify the electric-field-induced phase transformation in this material. The observed *111* reflection asymmetry and *200* reflection splitting reveal that the field-induced phase transformation for

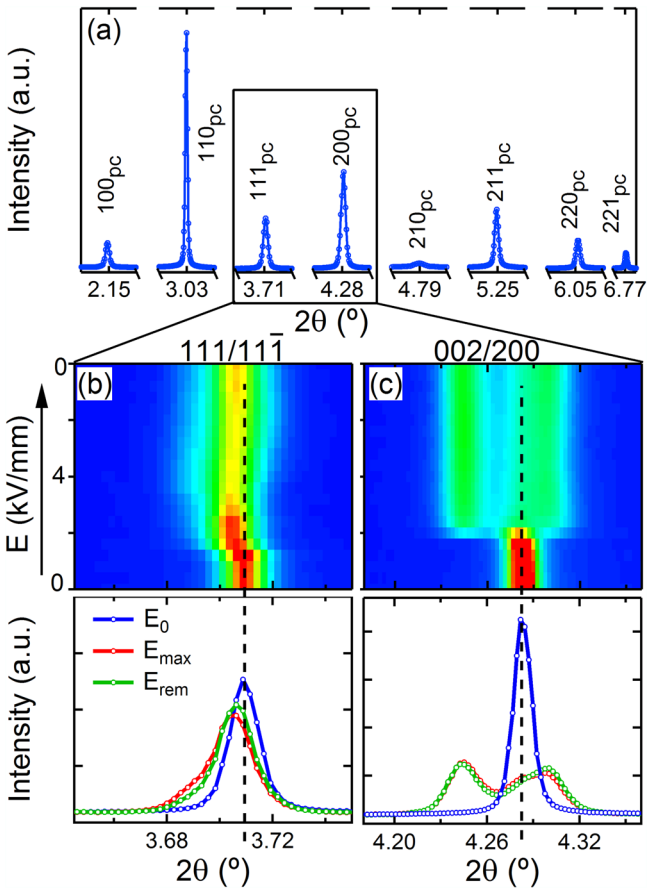

FIG. 1. (a) Diffraction profile for BNT-7BT in the as-processed state showing single and symmetric reflections consistent with a pseudocubic structure. (b) and (c) Variation in *111* and *200* reflections as a function of applied electric field up to 4 kV/mm. A change in as-processed state is initiated around ~1.2 kV/mm. Bottom of (b) and (c) shows the peak profiles in the as-processed state (E_0), at 4 kV/mm (E_{max}) and after the removal of the electric field (E_{rem}). The black dashed lines indicate the corresponding reflection positions in the as-processed pseudocubic BNT-7BT (i.e., at E_0). These data represent scattering information with applied electric field vector parallel to the scattering vector (i.e., $\psi = 0°$).

the BNT-7BT in this study is from pseudo-cubic to mixed rhombohedral and tetragonal symmetry, and is irreversible, consistent with earlier reports on morphotropic BNT-*100x*BT.[14,37] While the long range structure is cubic in the initial state, the relaxor-like[34] nature of the as-processed BNT-7BT signifies that the material contains disorder at the atomic or nanometer length scale which may be in the form of octahedral tilt disorder as well as cation occupational and displacement disorder.[35,38] Therefore, the nature of the electric-field-induced phase transformation in this material has been perceived as an establishment of long range ordering of the short range lower symmetries and simultaneous development of the corresponding lattice distortion with applied electric field.[39–41] In order to understand the thermodynamics of such transformations, the total free energy of any given crystallite within the polycrystalline material can be considered and written as a volume weighted sum of all the contributing factors[42]

$$F = \int_V (f_{bulk} + f_{elastic} + f_{electrostatic}) dV. \quad (1)$$

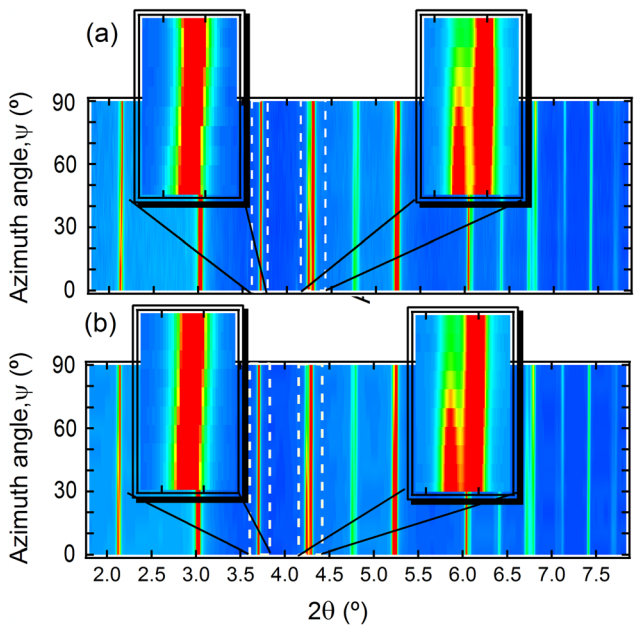

FIG. 2. Measured (a) and modelled (b) orientation dependent diffraction patterns at maximum field.

Here, the bulk free energy, f_{bulk}, can be expanded in terms of the polarisation order parameter.[43] The elastic energy, $f_{elastic}$, is related to the elastic stiffness and spontaneous strain, and the electric energy, $f_{electrostatic}$, is a combination of dipole-dipole interaction, depolarisation energy, and energy due to coupling with the applied electric field.

Particularly in the polycrystalline state, electrostatic and strain interactions not only occur within the crystallites themselves at ferroelectric domain boundaries but also these interactions at grain boundaries must be accounted for. Thus, upon expansion, coupling terms between strain and electrostatic interactions arise. In the case of a negative coupling parameter,[44] increase in strain energy, for example, results in a decrease in electrostatic energy to lower the total free energy of the system. Here, the electric field is considered to be the control parameter. Therefore, under an applied electric field, the changes in the order parameters for a given grain determine its resultant phase symmetry.

The mixed phase symmetry that results is likely due to the flattening of the total free-energy landscape as a function of crystal orientation relative to the applied field vector,[45] thus transformations to tetragonal or rhombohedral symmetry are possible with very small changes in bulk potential, f_{bulk}. The mixed phase symmetry of the material, however, will result in many possible polar directions, which may act to lower the electrostatic energy $f_{electrostatic}$, particularly at grain boundaries, thus making this the preferred phase structure in the current composition. Additionally, after the phase transformation has occurred, the distribution and the minimisation of elastic energy and electrostatic energy are also important to understand domain switching.[42] It is generally accepted that domain switching increases the elastic energy at the granular scale;[46] therefore, the reduction in electrostatic energy is also a driving force for domain switching.

From observations in Figure 1, it can be qualitatively stated that the macroscopic strain in BNT-7BT stems from lattice strain, domain switching, and a phase transformation. Electric-field-induced structural changes in morphotropic BNT-7BT have been extracted from diffraction data using full pattern Rietveld refinement incorporating full texture analysis. Figure 2 shows typical fitting of the measured diffraction profiles at E_{max}. The refinement with *R*3*c* and *P*4*mm* structure can model the measured field-induced data accurately. Related refinement parameters are listed in Table I. It is worthwhile to mention that upon field application in the poling cycle, the as-processed BNT-7BT remains pseudocubic up to fields of 1.2 kV/mm and was modelled using a single phase cubic $Pm\bar{3}m$ structure.

TABLE I. Refined structural parameters for both phases and criteria of fit for BNT-7BT at E_{max} (4 kV/mm). The V_{pc} indicate the unit cell volume of the pseudocubic primitive cell, and η is the lattice distortion.

	*R*3*c*	*P*4*mm*	Criteria of fit
a (Å)	5.52340(5)	3.89488(3)	R_{wp}: 0.04823
c (Å)	13.57163(4)	3.94424(5)	R_p: 0.031781
V_{pc} (Å^3)	59.79(3)	59.85(2)	
η(%)	0.342(3)	1.263(4)	
Fraction (%)	40.4(6)	59.6(5)	

By using this data analysis technique, lattice strain (ε^L), domain texture, and phase fraction for each phase at each field step is obtained. The ε^L (i.e., intrinsic contribution) was obtained from the WSODF strain model for the individual phases at each electric field step. On the other hand, the variation in relative intensity as a function ψ is a signature of non-180° ferroelectric domain texture. From the texture refinement with the orientation dependent diffraction data, the complete orientation distribution function (ODF) can be found and used to calculate the magnitude of texture along the polar axis in units of multiples of a random distribution (MRD). Using the obtained lattice distortion (η) and MRD, the domain switching strain (ε^D) can be calculated using the following equation:[20]

$$\varepsilon^D = \eta \frac{1}{2\pi} \int_{\alpha=0}^{\frac{\pi}{2}} \left[\Delta f_{hkl}(\alpha) \cos^2\alpha\right](\sin\alpha) d\alpha, \tag{2}$$

where $\Delta f_{hkl}(\alpha)$ is the change in MRD of the polar axis along the sample direction, α, with respect to the applied electric field vector. The lattice distortion is defined as $\eta_{Rh} = \sqrt{2}c_{Rh}/2\sqrt{3}a_{Rh} - 1$ and $\eta_{Tet} = c_{Tet}/a_{Tet} - 1$.[37]

In addition, the strain resulting from the electric-field-induced pseudocubic to rhombohedral-tetragonal phase transformation (ε^V) can be calculated from the volumetric change between the initial and resultant phases by the equation[47]

$$\varepsilon^V = \frac{1}{3}\left[\left\{(PF_{Rh} \times V_{Rh}) + (PF_{Tet} \times V_{Tet}) - V_{PC}\right\}/V_{PC}\right], \tag{3}$$

where V_{PC}, V_{Rh}, and V_{Tet} are the unit cell volumes of the pseudocubic, rhombohedral, and tetragonal phases, respectively. PF_{Rh} and PF_{Tet} are the phase fraction of the rhombohedral and tetragonal phases, respectively.

Change in phase fraction, unit cell volume, and related microscopic strain contributions calculated from the extracted refinement parameters as well as the measured macroscopic strain are shown in Figure 3.

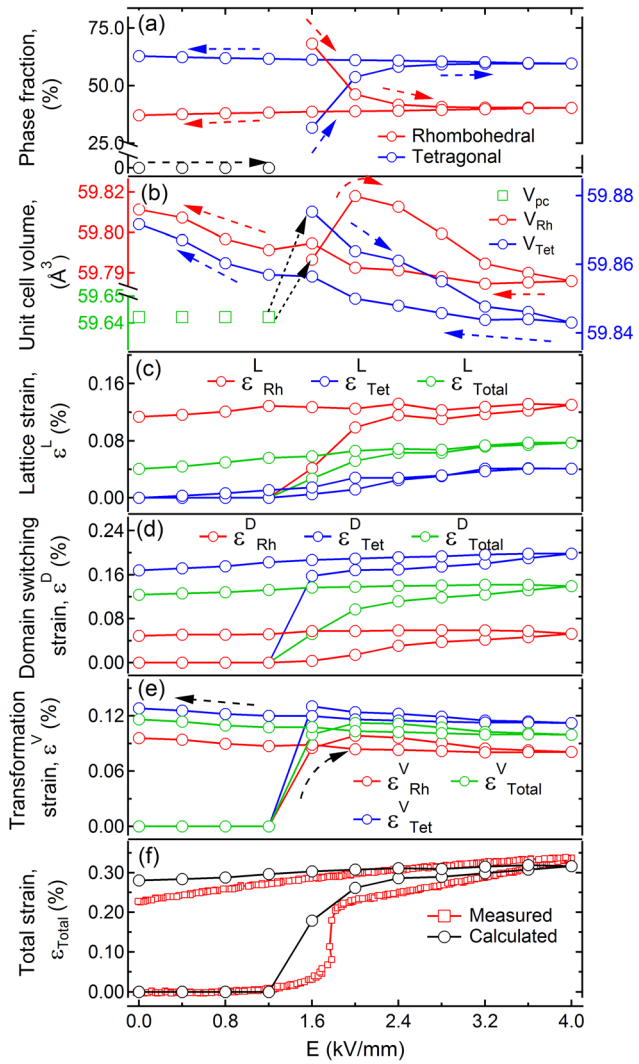

FIG. 3. Quantification of electric-field-induced (a) phase evolution, (b) change in unit cell volume, (c) lattice strain, (d) domain switching strain, (e) phase transformation strain, and (f) measured macroscopic strain and calculated total strain from diffraction data. ε_{Total} (green circles in (c)–(e)) is the strain value weighted with the phase fractions. The unit cell volume, V, in (b) represents unit cell volume of the pseudocubic primitive cell.

As can be seen from Figure 3(a), at the onset of pseudocubic to rhombohedral-tetragonal phase transformation, the major phase is rhombohedral $R3c$ (67%) and with increasing electric field, this fraction decreases. At an electric field of around 2 kV/mm, the composition is approximately an equal mixture of rhombohedral and tetragonal phases, and at the maximum field the tetragonal phase becomes the majority phase. From Figure 3(b), it is clear that the pseudocubic to mixed phase transformation initiates at 1.2 kV/mm. This is highlighted by changes in the unit cell volume, a result that is consistent with the previous report of electric-field-induced volume changes in BNT-*100x*BT compositions.[11]

Several observations can be made from the calculated ε^L, ε^D, and ε^V presented in Figures 3(c)–3(e). The ε^L contribution in the morphotropic BNT-7BT is mostly generated from the rhombohedral phase ($\varepsilon^L_{Rh} \approx 0.13\%$), and the ε^L_{Tet} is only about 0.04%. Whereas the ε^D is largely contributed by the tetragonal phase, i.e., $\varepsilon^D_{Tet}.(\sim 0.20\%) > \varepsilon^D_{Rh}$ ($\sim 0.05\%$). The transformation strain, ε^V, is slightly greater for the tetragonal phase. In the rhombohedral phase, the intrinsic (i.e., $\varepsilon^L_{Rh} = 0.13\%$) and extrinsic (i.e., combination of ε^D_{Rh} and ε^V_{Rh} is 0.13%) contributions are comparable. On the other hand, almost all of the contributions in the tetragonal phase stem from extrinsic processes, i.e., domain switching and phase transformation strain. The strain contribution from one switched domain is the difference of the c and a lattice parameters, i.e., η_{Tet} and η_{Rh} for tetragonal and rhombohedral, respectively. The higher degree of ε^D_{Tet} is directly related to the large η_{Tet} ($\sim 1.26\%$ at E_{max}) that is approximately four times greater than the η_{Rh} is $\sim 0.34\%$.[20] From the phase weighted calculated strain (green circles in Figures 3(c)–3(e)), it is evident that in the mixed phase BNT-7BT composition, extrinsic processes are the major contributors to the electric-field-induced strain, a result that is consistent with that reported for an MPB composition of $Pb(Zr,Ti)O_3$.[48,49]

The comparison of calculated total strain and measured macroscopic strain is shown in Figure 3(f). Within experimental errors, the strain calculated from the diffraction data (0.32%) is in agreement with the macroscopically observed strain response (0.34%). The measured macroscopic strain of this BNT-7BT is consistent with that of a previously reported value.[26] Differences between the calculated and observed macroscopic strain at other field strengths most likely arise from the time-dependence of the strain mechanisms. Zhou and Kamlah[50] have shown, in $Pb(Zr,Ti)O_3$-based materials, that creep occurs and is particularly large close to the coercive field. The difference in collection frequency, therefore, has a particularly strong effect on the observed coercive field and slopes of strain vs E curves.

Although the ε^L, ε^D, and ε^V contributions are determined individually and constitute the macroscopic strain response, they are not completely independent of each other. The origin of the strain in the poling cycle is essentially the electric-field-induced phase transformation. Unit cell volumes after the onset of phase transformation do not change significantly (Figure 3(b)). However, the rhombohedral phase fraction decreases and the tetragonal phase fraction increases (Figure 3(a)), thus it can be inferred that the ferroelectric domain switching is a possible contributor to the change in phase fraction, i.e., phase switching due to the coupling of strain from non-180° ferroelectric domain switching. Therefore, it can be stated that in this BNT-7BT composition both phase transformation (pseudocubic to lower symmetries) and phase switching (change in phase fraction between rhombohedral and tetragonal symmetry) are coupled. The sequence can be perceived as, at a certain critical field, the initial pseudocubic BNT-7BT transforms to the long range ferroelectric order with accompanying unit cell volume change where the major phase is rhombohedral. With further increase of the electric field, switching of ferroelectric domains drives the transformation of rhombohedral phase into tetragonal phase without any significant change in the unit cell volume.

The observed electric-field-induced phase transformation in BNT-7BT is irreversible. Therefore, the large fraction of phase transformation strain is only accessible for the poling cycle. Harnessing the ε^V can be critical to improve actuator properties of morphotropic BNT-7BT and other related compositions. Compositional modification of BNT-7BT has been reported previously to achieve this.[51,52] In these cases, a small fraction of sodium potassium niobate was used to tune the strain properties of mixed-phase BNT-*100x*BT, where the modified composition undergoes a

reversible electric-field-induced phase transformation without any significant remanent volume change.[53] The reversibility of the phase transformation also ensures that all strains associated with the formation and movement of non-180° ferroelectric domain walls are completely reversible. This behaviour is analogous to the shape memory effect in a super-elastic material, where large recoverable strains are achieved through a stress-induced martensitic transformation from a parent phase without a domain structure. Here, the zero field state is free from a domain structure, thus any strain generated from the formation and movement of domain walls by application of field is reversible if the phase transformation is also reversible upon removing that field.

In summary, by using full pattern Rietveld refinement of *in situ* high energy XRD data, we have quantified the microscopic strain contributions to the electric-field-induced strain in a morphotropic BNT-7BT. This quantitative analysis highlights the microscopic strain contributions in BNT-7BT during poling, finding 24%, 44%, and 32% of the total macroscopic strain is generated from lattice strain, domain switching, and phase transformation strain, respectively. Contributions from both rhombohedral and tetragonal phases in the morphotropic material have also been quantified as a function of applied electric field. The analysis of phase transformation behavior and related strain mechanisms indicates that to achieve high electric-field-induced strain for actuator application harnessing of the phase transformation strain is essential. This analysis of electric-field-induced strain will help develop strategies to further improve the properties of lead-free electroceramics through structural and/or chemical design.

This work was supported in part by the Australian Research Council Discovery Grant Nos. DP120103968 and DE150100750. J.E.D. acknowledged financial support from an AINSE research fellowship. Further funding has been received from the BMBF (Bundesministerium fuer Bildung und Forschung) (Grant No. 05K13VK1). This work was carried out with the support of the Diamond Light Source under the Experiment No. EE8019. C.G. acknowledges financial support from the state center AdRIA on adaptronics. W.J. wishes to acknowledge the financial support through the National Research Foundation of Korea (NRF) grant funded by the Korea government (MISP) (No. 2014R1A2A1A11053597).

[1]Y. Hiruma, H. Nagata, and T. Takenaka, J. Appl. Phys. **104**, 124106 (2008).
[2]Y. Hiruma, Y. Imai, Y. Watanabe, H. Nagata, and T. Takenaka, Appl. Phys. Lett. **92**, 262904 (2008).
[3]Y. Makiuchi, R. Aoyagi, Y. Hiruma, H. Nagata, and T. Takenaka, Jpn. J. Appl. Phys., Part 1 **44**, 4350 (2005).
[4]H. Nagata, M. Yoshida, Y. Makiuchi, and T. Takenaka, Jpn. J. Appl. Phys., Part 1 **42**, 7401 (2003).
[5]T. R. Shrout and S. J. Zhang, J. Electroceram. **19**, 113 (2007).
[6]T. Takenaka, K. I. Maruyama, and K. Sakata, Jpn. J. Appl. Phys., Part 1 **30**, 2236 (1991).
[7]R. Ranjan and A. Dviwedi, Solid State Commun. **135**(6), 394 (2005).
[8]C. Ma and X. Tan, Solid State Commun. **150**, 1497 (2010).
[9]W. Jo, J. E. Daniels, J. L. Jones, X. Tan, P. A. Thomas, D. Damjanovic, and J. Rödel, J. Appl. Phys. **109**, 014110 (2011).
[10]G. Picht, J. Töpfer, and E. Hennig, J. Eur. Ceram. Soc. **30**, 3445 (2010).
[11]W. Jo and J. Rödel, Appl. Phys. Lett. **99**, 042901 (2011).
[12]F. Cordero, F. Craciun, F. Trequattrini, E. Mercadelli, and C. Galassi, Phys. Rev. B **81**, 144124 (2010).
[13]J. E. Daniels, W. Jo, J. Roüdel, and J. L. Jones, Appl. Phys. Lett. **95**, 032904 (2009).
[14]H. Simons, J. Daniels, W. Jo, R. Dittmer, A. Studer, M. Avdeev, J. Rödel, and M. Hoffman, Appl. Phys. Lett. **98**, 082901 (2011).
[15]C. Ma, H. Guo, S. P. Beckman, and X. Tan, Phys. Rev. Lett. **109**, 107602 (2012).
[16]W. Jo, R. Dittmer, M. Acosta, J. Zang, C. Groh, E. Sapper, K. Wang, and J. Rödel, J. Electroceram. **29**, 71 (2012).
[17]H. Zhang, P. Xu, E. Patterson, J. Zang, S. Jiang, and J. Rödel, J. Eur. Ceram. Soc. **35**, 2501 (2015).
[18]M. Acosta, W. Jo, and J. Rödel, J. Am. Ceram. Soc. **97**(6), 1937 (2014).
[19]H.-S. Han, W. Jo, J.-K. Kang, C.-W. Ahn, I. W. Kim, K.-K. Ahn, and J.-S. Lee, J. Appl. Phys. **113**, 154102 (2013).
[20]J. L. Jones, M. Hoffman, and K. J. Bowman, J. Appl. Phys. **98**, 024115 (2005).
[21]A. Pramanick, J. E. Daniels, and J. L. Jones, J. Am. Ceram. Soc. **92**, 2300 (2009).
[22]A. Pramanick, D. Damjanovic, J. E. Daniels, J. C. Nino, and J. L. Jones, J. Am. Ceram. Soc. **94**, 293 (2011).
[23]H. Kungl, R. Theissmann, M. Knapp, C. Baehtz, H. Fuess, S. Wagner, T. Fett, and M. J. Hoffmann, Acta Mater. **55**, 1849 (2007).
[24]M. C. Ehmke, N. H. Khansur, J. E. Daniels, J. E. Blendell, and K. J. Bowman, Acta Mater. **66**, 340 (2014).
[25]M. Hinterstein, M. Hoelzel, J. Rouquette, J. Haines, J. Glaum, H. Kungl, and M. Hoffman, Acta Mater. **94**, 319 (2015).
[26]C. Groh, W. Jo, and J. Rödel, J. Appl. Phys. **115**, 234107 (2014).
[27]J. E. Daniels and M. Drakopoulos, J. Synchrotron Radiat. **16**, 463 (2009).
[28]J. L. Jones, A. Pramanick, and J. E. Daniels, Appl. Phys. Lett. **93**, 152904 (2008).
[29]J. E. Daniels, A. Pramanick, and J. L. Jones, IEEE Trans. Ultrason., Ferroelectr., Freq. Control **56**, 1539 (2009).
[30]A. P. Hammersley, S. O. Svensson, M. Hanfland, A. N. Fitch, and D. Hausermann, High Pressure Res. **14**, 235 (1996).
[31]S. Matthies, L. Lutteroti, and H. R. Wenk, J. Appl. Crystallogr. **30**, 31 (1997).
[32]S. Matthies, H.-R. Wenk, and G. W. Vinel, J. Appl. Crystallogr. **21**, 285 (1988).
[33]N. C. Popa and D. Balzar, J. Appl. Crystallogr. **34**, 187 (2001).
[34]W. Jo, S. Schaab, E. Sapper, L. A. Schmitt, H. J. Kleebe, A. J. Bell, and J. Rodel, J. Appl. Phys. **110**, 074106 (2011).
[35]J. E. Daniels, W. Jo, J. Rodel, D. Rytz, and W. Donner, Appl. Phys. Lett. **98**(25), 252904 (2011).
[36]D. Maurya, M. Murayama, A. Pramanick, W. T. Reynolds, K. An, and S. Priya, J. Appl. Phys. **113**, 114101 (2013).
[37]M. Hinterstein, L. A. Schmitt, M. Hoelzel, W. Jo, J. Rödel, H.-J. Kleebe, and M. Hoffman, Appl. Phys. Lett. **106**, 222904 (2015).
[38]J. Kreisel, P. Bouvier, B. Dkhil, P. Thomas, A. Glazer, T. Welberry, B. Chaabane, and M. Mezouar, Phy. Rev. B **68**, 014113 (2003).
[39]Y. Guo, Y. Liu, R. L. Withers, F. Brink, and H. Chen, Chem. Mater. **23**, 219 (2010).
[40]D. Maurya, A. Pramanick, M. Feygenson, J. C. Neuefeind, R. J. Bodnar, and S. Priya, J. Mater. Chem. C **2**, 8423 (2014).
[41]P. B. Groszewicz, H. Breitzke, R. Dittmer, E. Sapper, W. Jo, G. Buntkowsky, and J. Rödel, Phys. Rev. B **90**, 220104 (2014).
[42]S. Choudhury, Y. L. Li, C. E. Krill III, and L. Q. Chen, Acta Mater. **53**(20), 5313–5321 (2005).
[43]E. Salje and H. Zhang, Phase Transitions **82**(6), 452–469 (2009).
[44]E. K. Salje, *Phase Transitions in Ferroelastic and Co-elastic Crystals* (Cambridge University Press, 1991).
[45]D. Damjanovic, J. Am. Ceram. Soc. **88**(10), 2663–2676 (2005).
[46]L. Daniel, D. A. Hall, and P. J. Withers, Mech. Mater. **71**(0), 85–100 (2014).
[47]J. E. Daniels, W. Jo, J. Rödel, V. Honkimäki, and J. L. Jones, Acta Mater. **58**, 2103 (2010).
[48]M. J. Hoffmann, M. Hammer, A. Endriss, and D. C. Lupascu, Acta Mater. **49**, 1301 (2001).
[49]A. Endriss, M. Hammer, M. J. Hoffmann, A. Kolleck, and G. A. Schneider, J. Eur. Ceram. Soc. **19**, 1229 (1999).
[50]D. Zhou and M. Kamlah, Acta Mater. **54**, 1389 (2006).
[51]S. T. Zhang, A. B. Kounga, E. Aulbach, H. Ehrenberg, and J. Rödel, Appl. Phys. Lett. **91**, 112906 (2007).
[52]S. T. Zhang, A. B. Kounga, E. Aulbach, T. Granzow, W. Jo, H. J. Kleebe, and J. Rödel, J. Appl. Phys. **103**, 034107 (2008).
[53]W. Jo, T. Granzow, E. Aulbach, J. Rödel, and D. Damjanovic, J. Appl. Phys. **105**, 094102 (2009).